Inorganica Chimica Acta 469 (2018) 202–208

Contents lists available at ScienceDirect

Inorganica Chimica Acta

journal homepage: www.elsevier.com/locate/ica

Research paper

# Condensation product of 2-hydroxy-1-napthaldehyde and 2-aminophenol: Selective fluorescent sensor for $Al^{3+}$ ion and fabrication of paper strip sensor for $Al^{3+}$ ion

Smita Sarma [a], Ananya Bhowmik [b], Manas Jyoti Sarma [a], Sofia Banu [b], Prodeep Phukan [a], Diganta Kumar Das [a,*]

[a] Department of Chemistry, Gauhati University, Guwahati 781 014, Assam, India
[b] Department of Bio-engineering and Technology, Institute of Science and Technology, Gauhati University, Guwahati 781 014, Assam, India

ARTICLE INFO

*Article history:*
Received 2 June 2017
Received in revised form 8 September 2017
Accepted 10 September 2017
Available online 18 September 2017

*Keywords:*
2-Hydroxy-1-napthaldehyde
2-Aminophenol
Fluorescence
Sensor
Aluminium
PET
DFT-TDDFT
L6 myoblasts cell
Paper sensor

ABSTRACT

The condensation product of 2-hydroxy-1-napthaldehyde and 2-aminophenol (**L**), in 1:1 (*v/v*) $CH_3OH$: $H_2O$ acts as selective fluorescent sensor for $Al^{3+}$. The fluorescence intensity of **L** at emission wavelength 517 nm, when excited with 360 nm photons, increases on interaction with $Al^{3+}$ by *ca.* 7-fold. Under UV lamp, **L** shows light yellow fluorescence on interaction with $Al^{3+}$ visible to bare eyes. Metal ions – $Na^+$, $K^+$, $Ca^{2+}$, $Mg^{2+}$, $Mn^{2+}$, $Co^{2+}$, $Ni^{2+}$, $Cu^{2+}$, $Zn^{2+}$, $Pb^{2+}$, $Cd^{2+}$ and $Hg^{2+}$do not interfere. The increase in fluorescence intensity is due to the quenching of photoinduced electron transfer (PET) process prevailing in **L**. The fluorescent and UV/Visible spectral data analysis showed a 1:1 complexation between **L** and $Al^{3+}$ with $\log\beta = 4.532$ ($\beta$ = binding constant) and detection limit $10^{-5}$ M. DFT and TDDFT calculations also confirm 1:1 interaction between **L** and $Al^{3+}$. **L** has been successfully applied in fluorescent imaging of $Al^{3+}$ in live rat L6 myoblasts cells and as paper strip fluorescent sensor for $Al^{3+}$ in aqueous medium.



## 1. Introduction

In the earth crust, lithosphere consists of Aluminium (Al) in 8.3% which is considered to be third most abundant element after oxygen and silicon [1]. Aluminium compounds are widely used in textile industries, paper industries, in making utensils, in alloys [2], water purification, automobiles [3] etc. Due to its low density and therefore low weight, high strength, superior malleability, easy machining, excellent corrosion resistance, good thermal and electrical conductivity Al is the second most widely used metal after iron [4]. Although it is quite useful but it has got some adverse effects too. $Al^{3+}$ when consumed in surplus amount may lead to neurodegenerative disease like Alzheimer disease, Parkinson disease [5], bone abnormalities etc. Therefore the detection of $Al^{3+}$ is of great environmental as well as biological importance [6]. Fluorescent sensors have attracted a lot of scientific interest [7] due to their easy applicability, reasonable cost, higher sensitivity, simple instrumentation etc in comparson to other highly sophisticated techniques like atomic absorption and emission spectroscopy, spectrophotometry, electrochemistry, electrochemiluminescence etc [8,9].

As fluorescent sensor, simple Schiff base ligands, have gained recent interest for different metal ions including $Al^{3+}$. This is basically due to their relatively easy one or two steps synthesis [10–12]. Schiff bases recently reported as "off-on" fluorescent sensor for $Al^{3+}$ are based on – 2-Hydroxyacetophenone and ethylenediamine [13], thiazoleand salicylaldehyde [14]; 2-hydroxyethylether-2-nitrophenol and salicylaldehyde [15], 8-hydroxyjulolidine-9- carboxaldehyde and benzohydrazide [16]; 2-hydroxyaniline and 2 hydroxybenzaldehyde [17]; salicylhydrazide and ortho-phthalaldehyde [18]; salicylaldehyde and 4,4-difluoro-4-bora-3a,4adiaza-s-indacene [19]; thiophene-2-carboxylic acid hydrazide [20]; 8-hydroxyquinoline-7-carbal-dehyde and 4-aminopyrine [21]; 2-methyl quinoline-4-carboxylic hydrazide and 8-formyl-7-hydroxyl-4-methyl coumarin [22]; perylenebisimide and di(2-(salicylideneamino))ethylamine [23]; 4-aminoantipyrine and salicylaldehyde, 4-aminoantipyrine and 2-hydroxy-1 naphthaldehydeantipyridine [24]; Rhodamineethylenediamine and 1,8-naphthalic anhydride [25] etc.

* Corresponding author.
*E-mail address:* diganta_chem@gauhati.ac.in (D.K. Das).

https://doi.org/10.1016/j.ica.2017.09.025
0020-1693/

In this paper we have reported new fluorescent sensor for $Al^{3+}$ derived from the condensation of 2-hydroxy-1-napthaldehyde and 2-aminophenol in absolute alcohol. The sensor is selective for $Al^{3+}$ while metal ions – $Na^+$, $K^+$, $Ca^{2+}$, $Mg^{2+}$, $Mn^{2+}$, $Co^{2+}$, $Ni^{2+}$, $Cu^{2+}$, $Zn^{2+}$, $Pb^{2+}$, $Cd^{2+}$ and $Hg^{2+}$ do not interfere. The interaction of sensor with $Al^{3+}$ results bare eye visible light yellow fluorescence under UV lamp. The sensor is applicable to live rat L6 myoblasts cells and has been used to obtain paper strip fluorescent sensor for $Al^{3+}$ in aqueous medium.

## 2. Experimental

2-Hydroxy-1-napthaldehyde and DMSO-$d_6$ are from Sigma Aldrich, 2-aminophenol and metal salts were either from Merck or Loba Chemie. The metal salts except $Pb(NO_3)_2$, $CaCl_2$ and $HgCl_2$ were sulphates. Metal salt solutions (0.01M) were prepared in doubly distilled water obtained from quartz double distillation plant.

The FT-IR spectra were recorded in a Perkin Elmer RXI spectrometer as KBr pellets, NMR and $^{13}C$ NMR spectra were recorded on a Bruker Ultra Shield 300 MHz spectrophotometer using DMSO-$d_6$ as solvent. The fluorescence and UV/Visible spectra were recorded in HITACHI 2500 and Shimadzu UV 1800 spectrophotometer respectively using quartz cuvette (1 cm path length).

### 2.1. Synthesis and characterization of the sensor (L)

**L** has been reported as an intermediate towards the synthesis of a duel sensor for $Al^{3+}$ and $CN^-$ [26]. 0.02 mol (0.035 g) of 2-hydroxy-1-napthaldehyde and 0.02 mol (0.022 g) of 2-aminophenol were dissolved in 10 mL$C_2H_5OH$ in a 50 mL round bottom flask and allowed to stir for 8 h. Yellowish precipitate was obtained, solvent was evaporated in a rota evaporator to obtain the product which was recrystallized from $CH_3OH$. Yield: 70%.

**FTIR (**KBr**):**1592 $cm^{-1}$ ($\nu_{c=N}$); 3444 $cm^{-1}$ ($\nu_{o-H}$); 2922 $cm^{-1}$ ($\nu_{c-H\ aliphatic}$); 1512 $cm^{-1}$($\nu_{c=c}$).

**HRMS**: *m*/*z* 264.1.

**$^1$H NMR** (300MH$_z$, DMSO-$d_6$, δppm, TMS): 15.69 (d,***J*** = 9 Hz,1H); 10.38 (br,1H); 9.47 (d,***J*** = 9.6 Hz,1H); 8.36 (d,***J*** = 8.4 Hz,1H); 7.92 (d, ***J*** = 7.5 Hz,1H); 7.79 (d,***J*** = 9.6 Hz,1H); 7.66 (d,***J*** = 7.8 Hz,1H); 7.49–7.46 (m,1H); 7.27–7.25 (m,1H); 7.12–7.07 (m,1H); 6.99 6.93 (m,2H), 6.76 (d,***J*** = 9.3 Hz,1H).

**$^{13}$CNMR** (75 MHz, DMSO-$d_6$, δppm, TMS): 177.9, 149.4, 148.4, 138.1, 134.0, 129.1, 128.5, 128.2, 126.8, 125.9, 125.2, 123.1, 119.9, 119.8, 117.6, 116.0, 107.7.

### 2.2. Preparation of solutions

For sensing studies stock solution of **L** was prepared as $2 \times 10^{-5}$ M in 1:1 (*v*/*v*) $CH_3OH$:$H_2O$. Metal ions solutions were also prepared as 0.1 M in 1:1 (*v*/*v*) $CH_3OH$:$H_2O$. Fluorescent titrations were done by pipetting out 2 mL of solution of **L** in 1 cm quartz cell and by adding appropriate amount of metal ion using micro pipette. For reversibility studies the concentration of $EDTA^{2-}$ was made 0.1 M and added using micropipette.

### 2.3. DFT calculations

From the available experimental data the structure of **L**:$Al^{3+}$ complex was predicted and confirmed by DFT calculation. The **L** and **L**:$Al^{3+}$ complex were fully optimized using B3LYP [29] function. For **L** basis set 6-311G and for **L**:$Al^{3+}$ metal complex basis set LanL2DZ were used in the program Gaussian 09 [30]. The stability of the complex was confirmed by the vibrational energy calculation with same level of theory. TD-DFT calculations were performed to find out first three probable transitions of **L**:$Al^{3+}$ complex.

### 2.4. Cytotoxicity studies

To test the cytotoxicity of the compound 'A', a 3-(4,5-dimethylthiazol-2-yl)-2,Sdiphenyl tetrazolium bromide (MTT) assay was performed using the standard procedure. After treatment of the L6 cells with concentration ranging from (10–300) μM of compound A, 100 μl of MTT solution (5 mg $ml^{-1}$ phosphate-buffered saline (PBS) was added to each well of a 96-well culture plate and incubated continuously at 37 °C for 4 h. All the media was removed from the wells post incubation and replaced with 100 μl of DMSO for solubilising the blue-violet intracellular formazan crystals produced. Absorbance of the solution measured at 595 nm using a microtiter plate reader. The values obtained were the mean (±standard deviation) of three separate experiments. The cytotoxicity was calculated as a percentage of cell viability when compared to untreated control cells and expressed in terms of IC50.

## 3. Results and discussion

Scheme 1 A shows the chemical structure, based on different spectral data, of the synthesised sensor 1-((2-hydroxyphenylimino)methyl)naphthalene-2-ol (**L**). The DFT optimised structure of **L** has been shown in Scheme 1B.

The fluorescent spectrum of **L** ($2 \times 10^{-5}$ M) was recorded in 1:1 (*v*/*v*) $CH_3OH$:$H_2O$ with excitation wavelength 360 nm. The maximum emission peak was observed at $\lambda_{max}$value 517 nm. The fluorescence spectra of $2 \times 10^{-5}$ M solution of **L** was also recorded at different added concentrations of metal ions – $Na^+$, $K^+$, $Al^{3+}$, $Ca^{2+}$, $Mg^{2+}$, $Mn^{2+}$, $Co^{2+}$, $Ni^{2+}$, $Cu^{2+}$, $Zn^{2+}$, $Pb^{2+}$, $Cd^{2+}$ and $Hg^{2+}$. Significant enhancement in fluorescence intensity (*ca.* 7-fold) was observed only in case of $Al^{3+}$. Fig. 1 shows the fluorescence spectra of **L** in presence of different metal ions when metal ion to **L** concentration

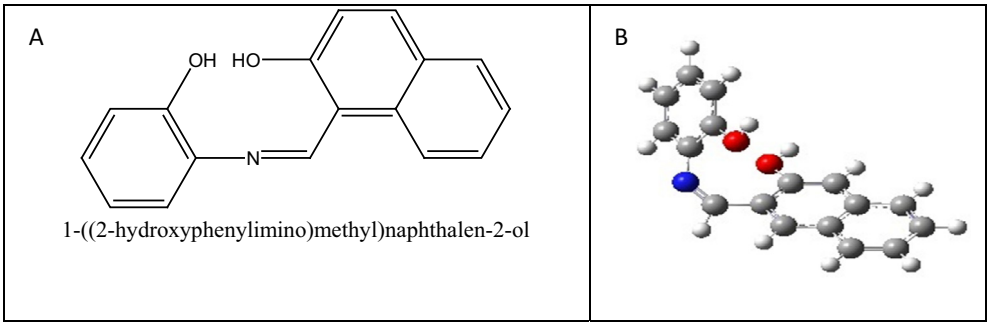


**Scheme 1.** Chemical structure of L (A) and DFT optimised structure of L (B).

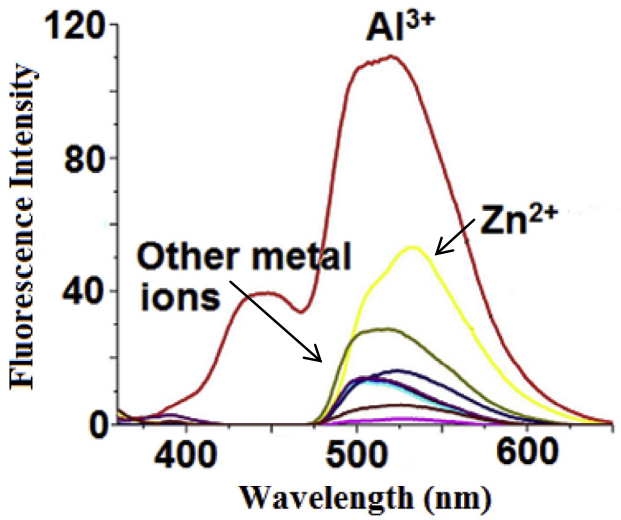


**Fig. 1.** Effect of different metal ions at one equivalent concentration on the fluorescence spectra of L in 1:1 (v/v) $CH_3OH:H_2O$ with $\lambda_{ex}$ = 360 nm.

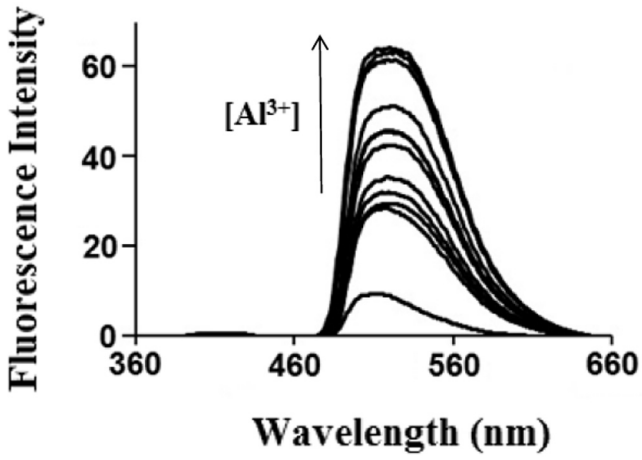


**Fig. 2.** Fluorescence spectra of L ($(2 \times 10^{-5}$ M) in 1:1 (v/v) $CH_3OH:H_2O$ at different added concentration of $Al^{3+}$, $\lambda_{ex}$ = 360 nm.

ratio is 1:2. Fig. 2 shows the fluorescence spectra of **L** in presence of different added concentrations of $Al^{3+}$. Inset of Fig. 2 is the plot of $I/I_0$ values for **L** versus concentration of added $Al^{3+}$ which attains maximum when $Al^{3+}$:**L** ratio became 1:1 indicating that one **L** binds per $Al^{3+}$. Here I and $I_0$ are the fluorescence intensity of **L** at two equivalent concentrations of a particular metal ion and in absence of $Al^{3+}$, respectively. The $I/I_0$ values for interaction between **L** and different metal ions mentioned above have been compared through a bar diagram in Fig. 3. Results shown in Fig. 1 and Fig. 3 clearly prove that **L** acts as a selective fluorescent sensor for $Al^{3+}$ over the other metal ions.

The enhancement in the fluorescence intensity of **L** on interaction with $Al^{3+}$ can be explained on the basis of Photo induced Electron transfer (**PET**) mechanism. The lone pairs of electrons in N and O atoms present on **L** are involved in PET causing quenching of fluorescence in it. When $Al^{3+}$ ion binds to **L** involving lone pairs on the N and O the PET was quenched and enhancement in the fluorescence intensity was observed.

The bare eye fluorescent recognition of $Al^{3+}$ by **L** was also possible when illuminated with UV radiation of 360 nm. Fig. 4 shows different solutions of **L** each in presence of a metal ion when **L** is in

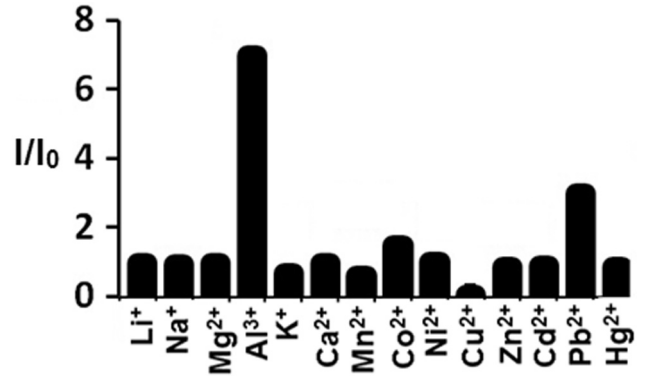


**Fig. 3.** Bar diagram comparing I/I0 values of L in presence of one equivalent of different metal ions in 1:1 (v/v) $CH_3OH:H_2O$, $\lambda_{ex}$ = 360 nm. The height of the bar corresponding to $Al^{3+}$ is distinctive over the others.

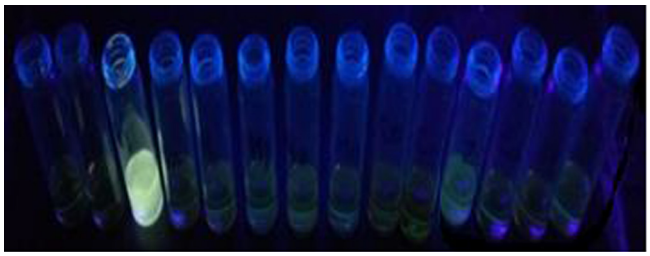

**Fig. 4.** Solutions of L each in presence of a metal ion (from left to right) – $Na^+$, $K^+$, $Al^{3+}$, $Li^+$, $Ca^{2+}$, $Mg^{2+}$, $Mn^{2+}$, $Co^{2+}$, $Ni^{2+}$, $Cu^{2+}$, $Zn^{2+}$, $Pb^{2+}$, $Cd^{2+}$ and $Hg^{2+}$ when L is in one equivalent to metal ion concentration in 1:1 (v/v) $CH_3OH:H_2O$, $\lambda_{ex}$ = 360 nm.

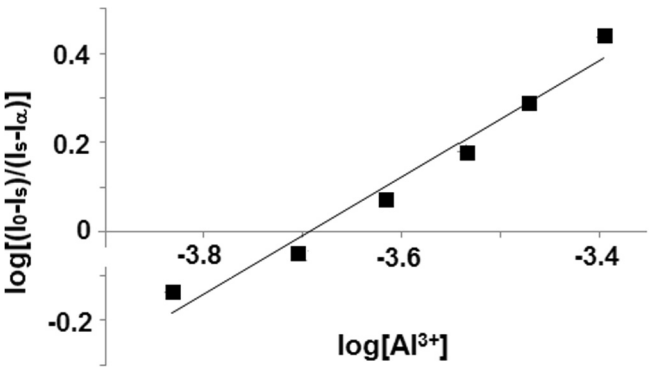


**Fig. 5.** Plot of $\log[(I0-Is)/(Is-I_\alpha)]$ versus $\log[Al^{3+}]$ for fluorescence spectral titration of L against $Al^{3+}$ in 1:1 (v/v) $CH_3OH:H_2O$, $\lambda_{ex}$ = 360 nm.

one equivalent to metal ion concentration. The solution containing $Al^{3+}$ fluoresces brightly under UV radiation of 360 nm wavelength while the other solutions do not.

The binding constant and stoichiometry of binding was determined by plotting $\log[(I_o-I_s)/(I_s-I_{max})]$ versus $\log[Al^{3+}]$ (Fig. 5) [27]. The slope of the plot was 1.2 indicating 1:1 binding ratio between **L** and $Al^{3+}$. The binding constant ($\beta$) has been calculated as $\log\beta = 4.5$. The binding stoichiometry as well as the binding constant was further confirmed by recording UV–visible spectra of **L** recorded at different added concentration of $Al^{3+}$ (Fig. 6) [27]. The two absorption peaks at 345 nm and 246 nm are due to $\pi$-$\pi^*$ transitions. Upon addition of $Al^{3+}$ absorption of both of these two peaks increases with the formation of three isosbestic points at 245 nm, 290 nm and 390 nm respectively. Inset of Fig. 6 is the plot of $\log[(A_o-A_s)/(A_s-A_{max})]$versus $\log[Al^{3+}]$. The slope 1.15 supports

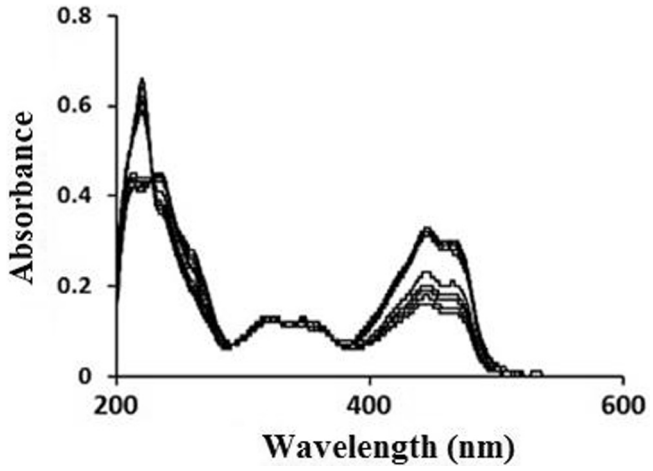


**Fig. 6.** UV/Visible spectra of L at different added concentration of $Al^{3+}$ in 1:1 (v/v) $CH_3OH:H_2O$.

the 1:1 interaction between **L** and $Al^{3+}$, the binding constant value has been calculated as logβ = 4.5 which is also in close proximity to the value calculated from fluorescence data. Here $I_0$ ($A_0$) is the fluorescence intensity (absorbance) of **L** in absence of metal ion, $I_s$ ($A_s$) is the fluorescence intensity (absorbance) of **L** in presence of a particular concentration of metal ion while $I_{max}$ ($A_\alpha$) is the maximum fluorescence intensity (absorbance) of **L** in presence of metal ion. The detection limit was calculated to be $10^{-5}$ M from the plot of ($I_s$-$-I_o$) versus log[$Al^{3+}$] as per reported procedure [28]. The Job's plot was also recorded to prove the 1:1 interaction between **L** and $Al^{3+}$ as shown in Fig. 7. The maximum absorbance at mole fraction 0.5 supports the 1:1 interaction.

The interference from other metal ions towards the sensing ability of **L** towards $Al^{3+}$ was verified. For this purpose, fluorescence spectra were recorded for **L** in presence of one equivalent of $Al^{3+}$ along with two equivalents of another metal ion. Fig. 8 compares $I/I_0$ values, through bar diagram, for **L** in presence of $Al^{3+}$ (black bars) along with **L** in presence of $Al^{3+}$ and another metal ion (grey bars). Here, $I_0$ is the fluorescence intensity of **L** in absence of any metal ion while I is the fluorescence intensity of **L**. The comparable heights of the black and grey bars indicate that **L** can detect $Al^{3+}$ even in presence of two equivalents of another metal ion.

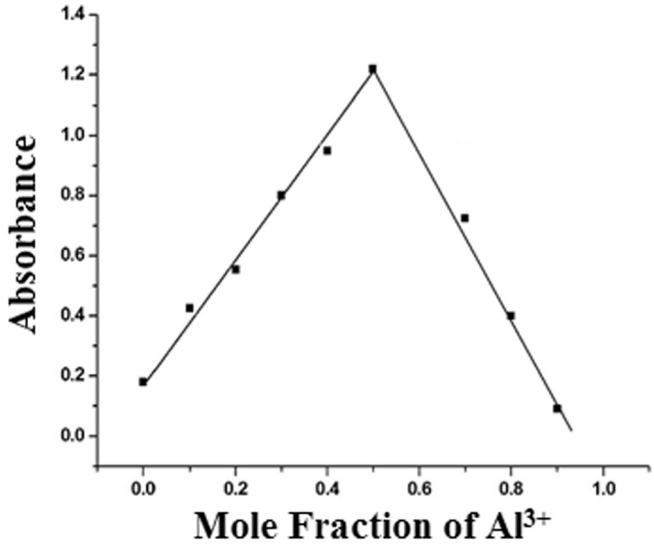


**Fig. 7.** Job's method of continuous variation for determining the stoichiometric binding ratio between L and $Al^{3+}$.

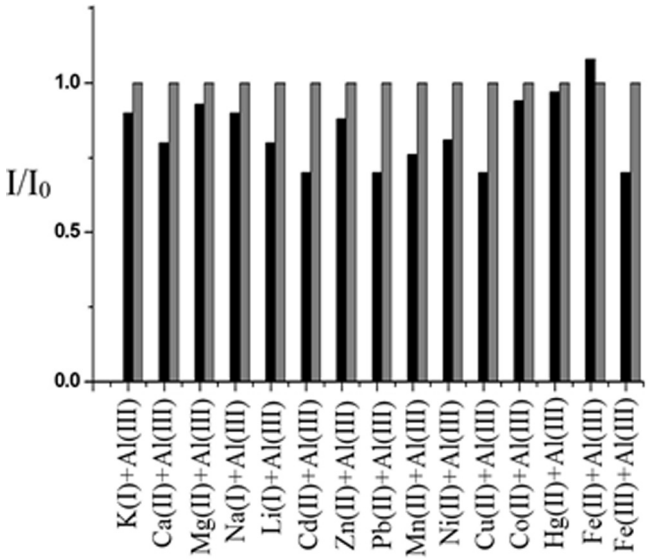


**Fig. 8.** I/I0 response of L in presence of (i) $Al^{3+}$ (grey bars); (ii) $Al^{3+}$ and another metal ion (black bars) in 1:1 (v/v) CH3OH:H2O. Similar heights of black and grey bars confirm selectivity of L towards $Al^{3+}$ over other metal ions.

### 3.1. Effect of pH on fluorescence of L in absence and presence of $Al^{3+}$

Fluorescence spectra of **L** as well as **L** in presence of one equivalent of $Al^{3+}$ were recorded varying the pH in the range 2.0–10.0 (Fig. 9). In case of **L** the fluorescence intensity remains almost same in the entire pH range. pH titration in presence of $Al^{3+}$ shows a gradual enhancement in fluorescence intensity till pH 6.0, remain constant until pH 8.0 is reached and then shows a gradual declination till pH 10.0. At pH lower than 6.0 the **L**:$Al^{3+}$ complex slowly breaks down due to the protonation of the two hydroxyl groups in L. Similarly above pH 8.0 the complex breaks down due to formation of aluminium hydroxide and declining fluorescence intensity is observed. Hence the **L**:$Al^{3+}$ complex remains stable in the pH range 6.0–8.0.

### 3.2. Reversibility with $Na_2EDTA$

The enhancement in the fluorescent intensity of **L** on interaction with $Al^{3+}$ was found to be reversible. When $Na_2EDTA$ was added

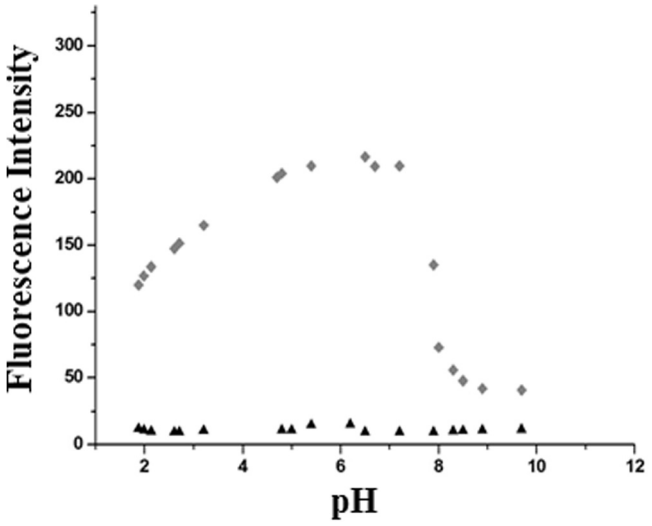


**Fig. 9.** Effect of pH on the fluorescent intensity of L (◆) and $Al^{3+}$:3 L (▲) in 1:1 (v/v) CH3CN:H2O.

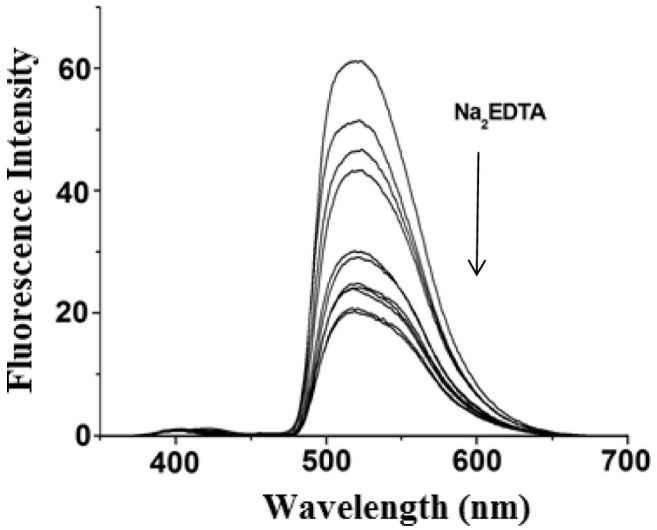


**Fig. 10.** Effect of EDTA2- anion at different added concentration on the fluorescence spectra of L in presence of one equivalent of $Al^{3+}$. The gradual decrease in fluorescence intensity proves the reversibility of $Al^{3+}$ to **L** binding.

gradually to an already fluorescent 1:1 equivalent solution of **L** and $Al^{3+}$, decrease in the fluorescence intensity was observed till it became equal to the original fluorescence intensity of **L** (Fig. 10). Here the strong chelator $EDTA^{2-}$ removes $Al^{3+}$ from **L**:$Al^{3+}$ complex as $[(EDTA)Al]^{-}$ and free **L** leaves behind.

### 3.3. DFT calculations

From the DFT optimized structure it has been seen that **L** is not fully planner, it has a twisted structure in the optimized form. Calculations show that **L**:$Al^{3+}$ complex has trigonal planner structure with $Al^{3+}$ at its centre (Fig. 11). In the optimized structure $Al^{3+}$ is bonded with two oxygen atoms and a nitrogen atom to complete its secondary valence. From optimized DFT structure it could be observed that, in the L:$Al^{3+}$ complex the π-electron cloud of naphthylene ring have been extended to the –C=N– imine bond through, the –CH link. Due to this extended delocalization of π-electron, fluorescence intensity might be enhanced in the L:$Al^{3+}$ complex compare to L. Moreover from DFT, optimized HOMO-LUMO of **L** and **L**:$Al^{3+}$ complex was calculated and it is observed that for **L**:$Al^{3+}$ complex HOMO is totally **L** centric (Fig. 12).

TD-DFT studies show that there are mainly three transitions (Hartree/Particle) for **L**:$Al^{3+}$ complex. The first transition is from HOMO (−0.24294) to LUMO (−0.13059), second one is from HOMO-1 (−0.25909) to LUMO and the third one is from HOMO to LUMO + 1 (−0.09821) and the last transition due to ligand to metal charge transfer.

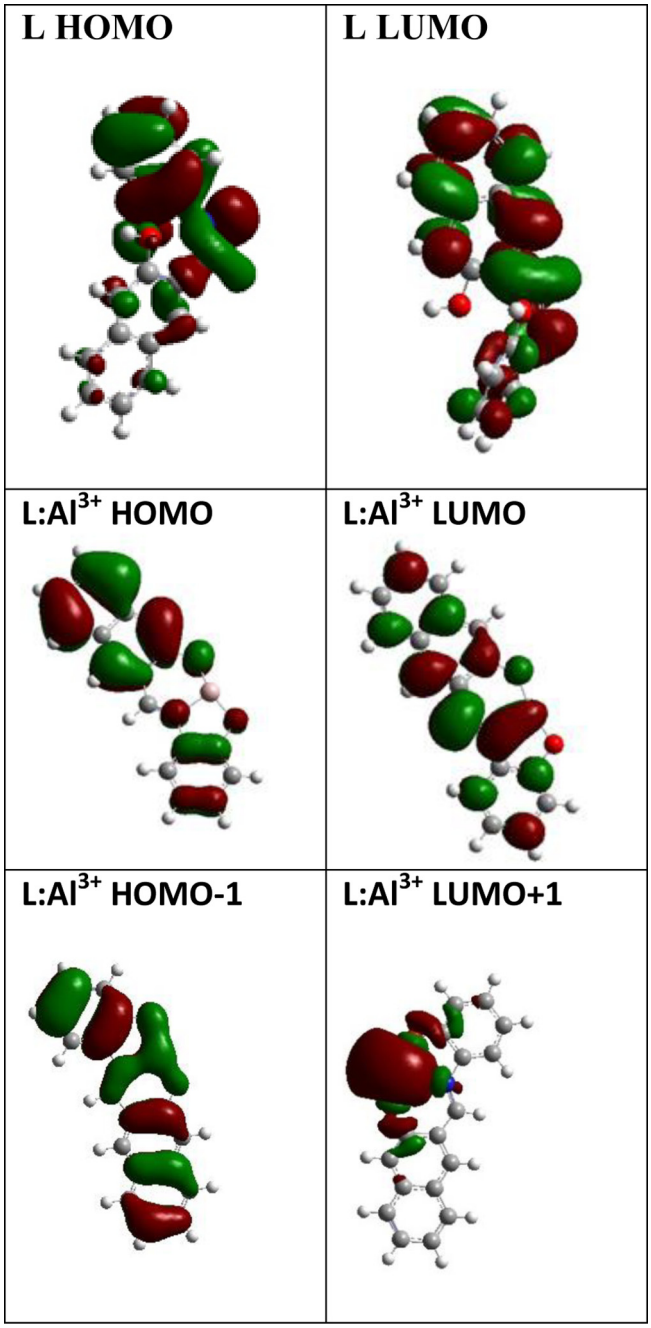


**Fig. 11.** DFT optimised structure of **L**:$Al^{3+}$ complex. $Al^{3+}$ binds to one N and two O atoms in a trigonal planar mode.

**Fig. 12.** DFT optimised shapes of HOMO & LUMO of L; HOMO, LUMO, HOMO-1 & LUMO + 1 of L:$Al^{3+}$.

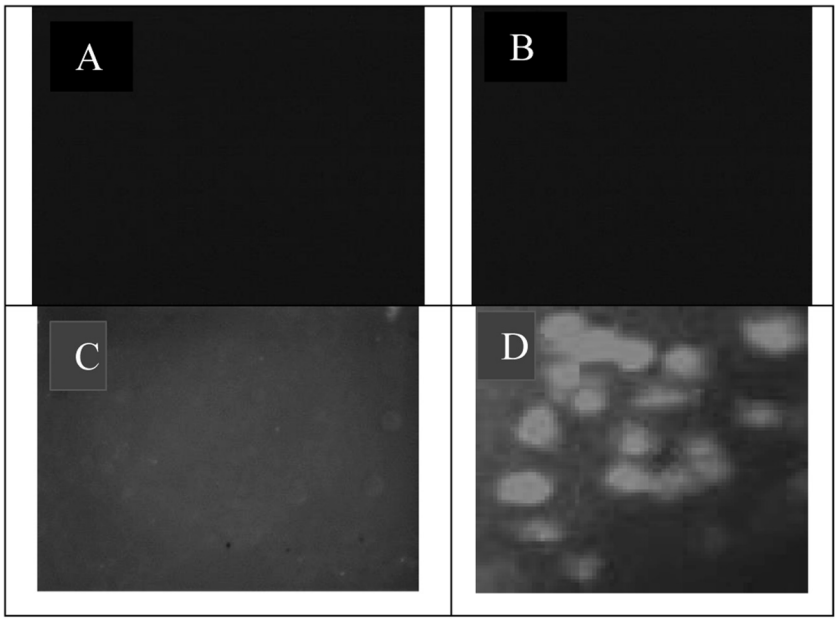


**Fig. 13.** Fluorescence image of (A) rat L6 myoblasts cells (B) Rat L6 myoblasts cells in presence of $Al^{3+}$ (C) Rat L6 myoblasts cells in presence of **L** (D) Rat L6 myoblasts cells in presence of **L** and $Al^{3+}$.

**Fig. 14.** Paper sensors for $Al^{3+}$ under UV light after interaction with $Al^{3+}$ (Left) and without interaction with $Al^{3+}$ (Right).

### 3.4. Living biological cell imaging studies

The biological application in case of **L** for sensing $Al^{3+}$ was done in rat L6 myoblasts which were grown in DMEM (Dulbecco's modified eaglemedium) supplemented with 10% Fetal Bovine Serum (FBS), 1% penicillin–streptomycin and maintained at 37 °C in a humidified atmosphere with 5% $CO_2$. 10 μL of aqueous $Al^{3+}$ was added and the cells were incubated for another 3 h. After completion of the incubation, the excess $Al^{3+}$ was washed with phosphate buffer saline (PBS). Then the fluorescence microscopy images were recorded for (A) Cells; (B) $Al^{3+}$ + Cells; (C) **L**+ Cells and (D) **L** + $Al^{3+}$ + Cells which were shown in (Fig. 13). The plate for **L** + $Al^{3+}$ + Cells shows bright spots which were not observed in case of other plates. This result confirms the applicability of **L** for fluorescence imaging of $Al^{3+}$ in live cells.

#### 3.4.1. Cytotoxicity Results

The MTT assay data signified that compound A was not greatly cytotoxic, with IC50 values of 300 ± 0.0015 μM in L6 cells. Hence, the concentration selected for our study was 50 μM which indicated 70 percent survival.

#### 3.4.2. Fluorescent paper sensor for $Al^{3+}$

1 mM solution of **L** prepared by dissolving appropriate amount of **L** in 1:1 (*v*/*v*) $CH_3OH$:$H_2O$. Whatmann 42 filter paper was cut in as 0.5 cm by 3 cm paper strip and placed on a clean and dry glass surface. The above solution of **L** was spread on 0.5 × 2 cm area of the paper strip carefully and allowed to dry normally. The process was repeated three times to obtain the paper strip fluorescent sensor for $Al^{3+}$. The coated portion of the paper strip was dip for 3 s into a solution of $10^{-5}$ M $Al^{3+}$ containing all the other metal ions studied above for interference keeping the concentration of each of them at $10^{-3}$ M. The strip is then dried under normal environment and placed under UV lamp to observed bright yellow-green fluorescence (Fig. 14).

## Acknowledgements

The DST, New Delhi and UGC, New Delhi are thanked for financial assistance to the Department through FIST and SAP respectively. IIT-Guwahati is thanked for HRMS. DST-SERB is thanked for financial assistance vide project No. EMR/2016/001745.

## Appendix A. Supplementary data

Supplementary data associated with this article can be found, in the online version, at http://dx.doi.org/10.1016/j.ica.2017.09.025.

## Reference

[1] B.K. Datta, C. Kar, A. Basu, G. Das, Tetrahedron Lett. 54 (2013) 771.
[2] Y.W. Choi, G.J. Park, Y.J. Na, H.Y. Jo, S.A. Lee, G.R. You, Sens. Actuator B 194 (2014) 343.
[3] N. Mergu, A.K. Singh, V.K. Gupta, Sensors 15 (2015) 9097.
[4] S.V. Verstraeten, L. Aimo, P.I. Oteiza, Arch. Toxicol. 82 (2008) 789.
[5] V. Kumar, A. Kumar, U. Diwan, Shweta Ramesh, S.K. Srivastava, K.K. Upadhyay, Sens. Actuator B 207 (2015) 650.
[6] S. Sarma, P.K. Bhattacharyya, D.K. Das, J. Fluoresc. 25 (2015) 1537.
[7] A. Sahana, A. Banerjee, S. Das, S. Lohar, D. Karak, B. Sarkar, S.K. Mukhopadhyay, A.K. Mukherjee, D. Das, Org. Biomol. Chem. 9 (2011) 5523.
[8] D. Brian, M.S. Brooks, M.M. Richter, Anal. Chem. 75 (2003) 1102.

[9] V.K. Gupta, A.K. Jain, G. Maheshwari, Talanta 72 (2007) 1469.
[10] K. Dutta, R.C. Deka, D.K. Das, J. Lumin. 148 (2014) 325.
[11] J. Kumar, M.J. Sarma, P. Phukan, D.K. Das, Dalton Trans. 44 (2015) 4576.
[12] J. Kumar, P. Bhattacharyya, D.K. Das, Spectrochim. Acta A 138 (2015) 99.
[13] D.K. Das, J. Kumar, A. Bhowmick, P.K. Bhattacharyya, S. Banu, Inorg. Chim. Acta 462 (2017) 167.
[14] V.K. Gupta, A.K. Singh, L.K. Kumawat, Sens. Actuators B 195 (2014) 98.
[15] C.H. Chen, D.J. Liao, C.F. Wan, A.T. Wu, Analyst 138 (2013) 2527.
[16] S.A. Lee, G.R. You, Y.W. Choi, H.Y. Jo, A.R. Kim, I. Noh, S.J. Kim, Y. Kim, C. Kim, Dalton Trans. 43 (2014) 6650.
[17] S. Kim, J.Y. Noh, K.Y. Kim, J.H. Kim, H.K. Kang, S.W. Nam, S.H. Kim, S. Park, C. Kim, J. Kim, Inorg. Chem. 51 (2012) 3597.
[18] L. Wang, W. Qin, X. Tang, W. Dou, W. Liu, Q. Teng, X. Yao, Org. Biomol. Chem. 8 (2010) 3751.
[19] R. Kang, X. Shao, F. Peng, Y. Zhang, G.T. Sun, W. Zhaoa, X.D. Jiang, RSC Adv. 3 (2013) 21033.
[20] K. Tiwari, M. Mishra, V.P. Singh, RSC Adv. 3 (2013) 12124.
[21] L. Fan, X. Jiang, B. Wang, Z. Yang, Sens. Actuators B 205 (2014) 249.
[22] J. Qin, T. Li, B. Wang, Z. Yang, L. Fan, Spectrochim. Acta A 133 (2014) 38.
[23] S. Malkondu, Tetrahedron 70 (2014) 5580.
[24] V.K. Gupta, A.K. Singh, N. Mergu, Electrochim. Acta 117 (2014) 405.
[25] S. Paul, A. Manna, S. Goswami, Dalton Trans. 44 (2015) 11805.
[26] Chang Ya-Ju, Wu Shih-Sheng, Hu Ching-Han, Cho Chien, Kao Min Xiu, Wu An-Tai, Inorg. Chim. Acta 432 (2015) 25.
[27] K. Dutta, R.C. Deka, D.K. Das, Spectrochim. Acta. A 124 (2014) 124.
[28] S. Sarma, P.K. Bhattacharyya, D.K. Das, J. Fluoresc. 26 (2016) 899.
[29] (a) A.D. Becke, J. Chem. Phys. 98 (1993) 5648;
(b) C. Lee, W. Yang, R.G. Parr, Phys. Rev. B 37 (1988) 785.
[30] M.J. Frisch, G.W. Trucks, H.B. Schlegel, G.E. Scuseria, M.A. Robb, J.R. Cheeseman, G. Scalmani, V. Barone, B. Mennucci, G.A. Petersson, H. Nakatsuji, M. Caricato, X. Li, H.P. Hratchian, A.F. Izmaylov, J. Bloino, G. Zheng, J.L. Sonnenberg, M. Hada, M. Ehara, K. Toyota, R. Fukuda, J. Hasegawa, M. Ishida, T. Nakajima, Y. Honda, O. Kitao, H. Nakai, T. Vreven, J. A. Montgomery, Jr., J.E. Peralta, F. Ogliaro, M. Bearpark, J.J. Heyd, E. Brothers, K.N. Kudin, V.N. Staroverov, T. Keith, R. Kobayashi, J. Normand, K. Raghavachari, A. Rendell, J.C. Burant, S.S. Iyengar, J. Tomasi, M. Cossi, N. Rega, J. M. Millam, M. Klene, J.E. Knox, J.B. Cross, V. Bakken, C. Adamo, J. Jaramillo, R. Gomperts, R.E. Stratmann, O. Yazyev, A. J. Austin, R. Cammi, C. Pomelli, J.W. Ochterski, R.L. Martin, K. Morokuma, V.G. Zakrzewski, G.A. Voth, P. Salvador, J.J. Dannenberg, S. Dapprich, A.D. Daniels, O. Farkas, J.B. Foresman, J.V. Ortiz, J. Cioslowski and D.J. Fox, Gaussian Inc, Wallingf, Gaussian 09, Revision B.01.